# Design and demonstration of a switching engine for a binary true-time-delay device that uses a White cell

Richard Higgins, Niru K. Nahar, and Betty Lise Anderson

Optical true-time-delay devices based on the White cell can be divided into two general types: polynomial cells, in which the number of delays that can be obtained is related to the number of times $m$ that a beam bounces in the cell raised to some power, and exponential cells, in which the number of delays is proportional to some number raised to the power of $m$. In exponential cells, the topic to be addressed, the spatial light modulator switches between a delay element and a null path on each bounce. We describe an improved design of this switching engine, which contains a liquid-crystal switch and a White cell. We examine astigmatism and corrections for it and present a specific design. © 2003 Optical Society of America

*OCIS codes:* 280.5110, 070.1170, 200.4740, 220.1000, 230.3720.

## 1. Introduction

Devices that produce optical true-time delays (OTTDs) can be used for the steering of radar phased arrays,[1] transversal filtering,[2,3] and other optical signal-processing applications. For radar applications, the two most important figures of merit are the number of delays that can be produced, which should be in the hundreds or thousands, and the number of antenna elements that can be supported, which may be from a few elements to tens of thousands. The number of delays that can be produced determines the resolution with which the beam can be steered, and the number of elements in the array determines the beam shape and quality.

In an OTTD there is one light beam per antenna element. The rf signal coming from (in receive mode) or going to (in transmit mode) a given antenna element is modulated onto the light beam. That light is then directed into paths of varying lengths to produce the controllable delays. Thus, to control a large array, one needs a device capable of independently switching a large number of optical beams among a large number of different paths.

Our approach to this problem is based on the White cell.[4,5] The White cell is an arrangement of mirrors that can provide multiple bounces for a large number of input beams, and the beams are refocused on every bounce. Each beam forms a unique set of spots, the number of spots being equal to the number of passes. We place a spatial light modulator (SLM) in the plane of the spots and thus are able to switch each beam on each bounce. We switch between paths of varying lengths to produce the delays.

We have previously reported several designs for White cell–based OTTDs. These can be categorized as polynomial cells or exponential cells. In polynomial cells the SLM switches beams between White cells of varying lengths on each pass.[6,7] The number of delays is proportional to the number of bounces $m$ raised to some power. In exponential cells the White cells are of the same length, but on each bounce the SLM switches the beam to a delay engine or a null path.[8] Now the number of delays is proportional to some base number raised to the power of $m$. A binary cell is one in which the number of delays grows as $2^m$.

In this paper we report on an improved design for the switching engine of a binary OTTD device. This new configuration uses fewer components than our earlier design used. We also discuss the effects of astigmatism and how to correct for them.

We begin by quickly reviewing the operation of the

R. Higgins is with Optimer Photonics, 505 King Avenue, Columbus, Ohio 43201. N. K. Nahar and B. L. Anderson (anderson@ee.eng.ohio-state.edu) are with The Ohio State University, 205 Dreese Laboratory, 2015 Neil Avenue, Columbus, Ohio 43210.

Received 3 December 2002.
0003-6935/03/234747-11$15.00/0

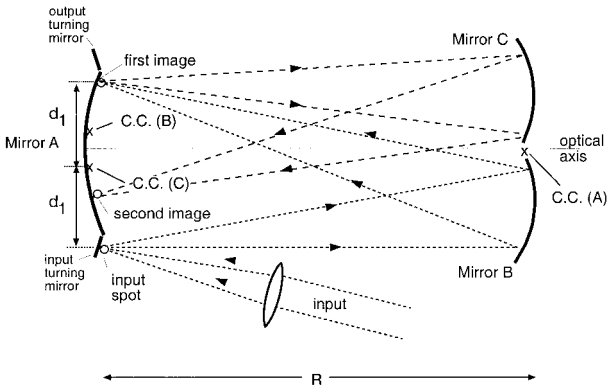


Fig. 1. Original White cell consists of three spherical mirrors, of identical radii of curvature $R$, separated by $R$. The centers of curvature (C.C.) for each mirror are shown. A spot introduced into the White cell via the input turning mirror produces a series of spots on mirror A.

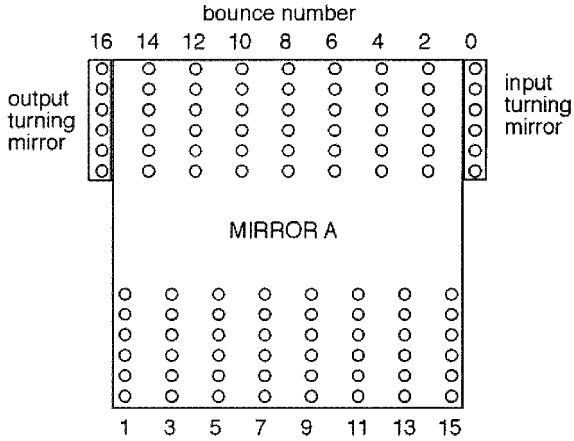


Fig. 2. Spot pattern produced on mirror A by six input beams undergoing 16 bounces apiece.

earlier binary true-time-delay (TTD) White cell device in Section 2. In Section 3 we discuss the new configuration and its design. In Section 4 we explore causes and severity of the astigmatism and suggest corrective action. Section 5 describes a specific design, and a summary and discussion are given in Section 6.

## 2. Binary True-Time-Delay Device Based on the White Cell

In this section we will introduce the original binary White cell TTD device. To that end, we will first discuss the White cell and then show how it is adapted to perform time-delay functions.

### A. Operation of the White Cell

The binary OTTD cell is based on the White cell (Fig. 1), which is a system of three spherical mirrors that have identical radii of curvature.[4,5] Mirror A is at the left, and two mirrors, B and C, are on the right. We have discussed the operation of the original White cell in some detail previously,[9] so here we summarize the key points. A beam is introduced into the White cell via an input turning mirror, shown at the bottom left. The light then goes to mirror B, which reimages the input spot onto mirror A. Thus the beam strikes the first location on mirror A. Next, mirror A reimages the light from B onto C. This second condition is an important feature of the White cell—because of the repeated imaging back and forth between B and C, there are no additional diffraction losses or truncations. Meanwhile, the first spot on mirror A is imaged by C onto a second spot on mirror A, and the process continues. The number of spots (bounces) is determined by the locations of the centers of curvature of mirrors B and C. This is another nice feature of the White cell. If mirrors B and C are aligned such that the last spot lands in the proper place, then *all* the spots are aligned in the proper places.

A third feature of the White cell is that many beams can circulate in the cell independently. Figure 2 shows the spot pattern that is made on mirror A when six input beams are circulating in the White cell and making 16 bounces. The spot pattern has also been discussed in detail previously.[9] Here we make the following observations:

1. Each beam strikes a unique set of spots on mirror A. When we adapt the White cell to time delay, we will replace mirror A with a pixelated SLM. Then each spot will land on a separate pixel.
2. A large number of spots can circulate in the White cell simultaneously. This number can be in the hundreds or thousands.
3. The spots enter via an input turning mirror and exit the cell via an output turning mirror. It is also possible to arrange the spots such that the exit bounces are on the same side of mirror A.
4. The odd-numbered bounces are on the bottom of the mirror, and the even-numbered bounces are on the top half of the mirror.

### B. Original White Cell–Based Binary Optical True-Time-Delay Device

Now we adapt the White cell to TTD. The original binary cell architecture is described in Ref. 8. We will summarize it briefly here for the convenience of the reader. Mirror A is first split into two parts, one for the odd bounces and one for the even bounces. Next, we replace the lower part, where the odd bounces land, with a SLM, in this case, a liquid-crystal type. This SLM and the flat mirror, called an auxiliary mirror, are shown at the left in Fig. 3. We add a polarizing beam splitter to allow us to change the path of the beams on the basis of their polarization state and a field lens to provide the imaging action of the previously spherical mirror A. This lens, in combination with the SLM and the auxiliary mirror, forms a White cell with mirrors B and C. There is a second White cell, formed by the SLM and mirrors E and F. Light is directed to E by the po-

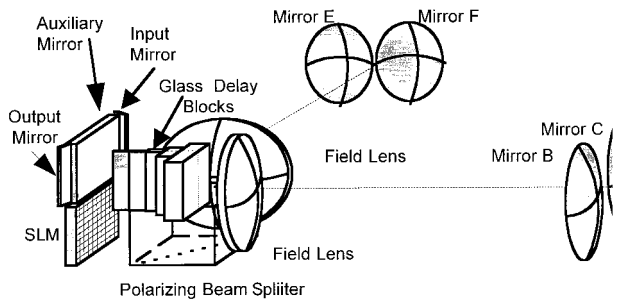


Fig. 3. Three-dimensional view of the TTD White cell with a binary architecture that uses glass blocks.

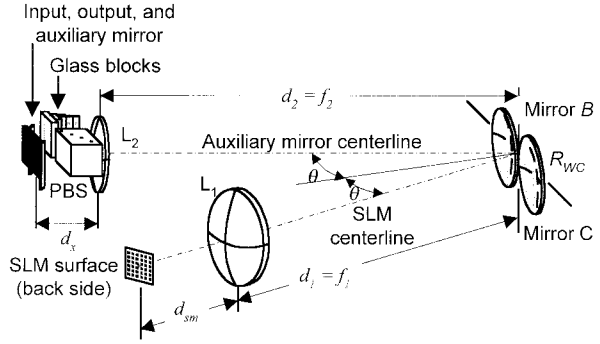


Fig. 4. Three-dimensional view of the new binary cell configuration. PBS, polarizing beam splitter.

larizing beam splitter when the polarization state of the beam is changed by the SLM. This could happen on any even bounce.

Because of the right-angle turn in the second White cell, when light goes to the EF White cell, the odd spots are formed in a plane conjugate to the flat mirror, but at right angles to it, and above the beam splitter. In the figure some glass blocks are shown in this location. These are the delay elements. Other delay mechanisms are also possible.[8] The glass blocks are reflective on the side toward the viewer in the figure, so that light entering a glass block returns to the White cell.

The operation of the cell is as follows. Light beams are introduced into the cell via the input turning mirror. They go to mirror B and then form a first column of spots on the SLM. The polarization of each beam can be independently changed at this point. Those that are polarized such that their light passes through the beam splitter travel to mirror C and form their second spots on the flat mirror. Those whose polarization is opposite will be reflected by the beam splitter, sent to mirror F, go through some particular glass block, and form spots on the back surface of the first glass block. It is beyond the scope of this paper to discuss these delay elements in detail; briefly, however, each glass block has a refractive index $n$ and thus slows the light down from its vacuum velocity. It also causes the spots to form in a plane slightly behind the plane equivalent to the flat mirror. In Ref. 8 it was shown how to choose the length and locations of the glass blocks to produce the proper time delay $\Delta$. Thus those beams that are switched on the first bounce experience a delay of $\Delta$ relative to the unswitched beams. Switched or not, all beams return to the SLM, and each one lands in the appropriate location of column 2 regardless of which White cell it returns from. This happens because the centers of curvature of mirrors E and F are coaligned with the centers of curvature of B and C, respectively. The bounce process continues.

Each glass block is twice the optical length of the one before it. The number of blocks is equal to the number of bits of delay that can be obtained. If a beam is sent to the flat mirror on every bounce, it requires some time $T_0$ to traverse the White cell and exit. If a beam is sent to the first glass block only, it accrues a delay of $T_0 + \Delta$, where $\Delta$ is the time increment. If it goes to the second block only, it gets delayed by $T_0 + 2\Delta$. A delay of $T_0 + 3\Delta$ is obtained when a beam goes to both the first and the second glass blocks, and so on. Note that the delay $T_0$ is common to all beams regardless of their paths, so it has no effect on the radar beam direction. The delay increment $\Delta$ is the *difference* between the path to the flat mirror and the path through the glass blocks, so this difference can be short or long.

If there are $m$ bounces, there are $m/2$ glass blocks, and the maximum time delay that can be obtained is

$$T_{\max} = 2^{m/2}. \tag{1}$$

There is a limit to how long a glass block can be before its width starts to truncate the beam. For long delays, one can use a lens train with mirrors in the corresponding column at various planes along the train.[8]

### 3. New Binary True-Time-Delay Switching Engine Using a White Cell

#### A. New Architecture

In this subsection we show that it is possible to reduce the number of components in the device of Fig. 3 while maintaining the same capability. Because the mirror pairs B and C and pairs E and F are identical, one can eliminate one set of mirrors by relocating the polarizing beam splitter. This is shown in Fig. 4. Here the auxiliary mirror and the beam splitter are moved away from the SLM. The main axis of the device goes from the SLM, through lens $L_1$ to the plane containing mirrors B and C, and then to the beam splitter and auxiliary mirror or delay element.

In operation, all the beams from the SLM propagate to mirror B and are reflected toward the beam splitter regardless of polarization. The beams are then either transmitted or reflected by the internal polarizing surface of the beam splitter. Depending on the polarization, beams either are transmitted and travel to the flat auxiliary mirror or are reflected and travel toward and enter the glass blocks to accumulate delay. As in the original design, the beams in-

side the glass blocks are internally reflected and double back to the beam splitter. All the beams then return to the SLM via mirror C for the next bounce.

With this new binary cell configuration, we have eliminated two spherical mirrors. An additional advantage is that the image of the SLM pixels can easily be magnified on the auxiliary focal plane and on the glass blocks. This enables one to implement longer delays in the glass blocks: The spots are magnified, so the beams corresponding to them diverge less. Thus a block of a given width can be longer before it begins to truncate the diverging beams. Furthermore, because the block width is equal to the pixel pitch, when the SLM plane is magnified, this pitch is increased too, further increasing the length of the time delays that can be realized.

### B. Imaging Equations

The new configuration of the binary cell must still satisfy the equivalent imaging requirements of the original White cell in order to maintain the predicted spot pattern. Using ray-matrix algebra, we derive three basic imaging conditions required to create this spot pattern.

The first condition in a White cell is that mirror A (Fig. 1) must image back onto itself through mirror B and also through mirror C. Here this condition takes the form that the SLM must image onto the auxiliary mirror through mirror B and that the auxiliary mirror must image onto the SLM through mirror C. By writing the paraxial ray matrices for each optical element in these paths and setting the B element of the result to zero to require imaging, we find that the distance $d_{\mathrm{sm}}$ between the SLM and lens $L_1$ is given as

$$d_{\mathrm{sm}} = \frac{f_1}{{f_2}^2 R_{\mathrm{WC}}} (f_1 f_2 R_{\mathrm{WC}} - f_1 d_{\mathrm{aux}} R_{\mathrm{WC}} - 2 f_1 {f_2}^2 + {f_2}^2 R_{\mathrm{WC}}), \tag{2}$$

where $R_{\mathrm{WC}}$ is the radius of curvature of mirrors B and C and $d_{\mathrm{aux}}$ (not shown in the figure) is the equivalent distance (correcting for the refractive index of the beam splitter) between the auxiliary focal plane and lens $L_2$. The focal lengths of lenses $L_1$ and $L_2$ are given by $f_1$ and $f_2$, respectively.

The second and third imaging conditions are that mirror B must image onto mirror C through the auxiliary mirror and that C must image onto B via the SLM. These conditions are required to ensure that the beam stays in the cell after successive bounces. This results in the focal lengths of the lenses being equal to the distance between that particular lens and the White cell mirrors:

$$d_1 = f_1, \tag{3}$$

$$d_2 = f_2. \tag{4}$$

These conditions and results are discussed in more detail in Refs. 6 and 8.

Using ray-matrix algebra, the magnification $M$ of the spots on the SLM to the auxiliary focal plane is

$$M = (f_2/f_1). \tag{5}$$

## 4. Astigmatism in New Binary True-Time-Delay White Cell

In any physical imaging system, aberrations will exist to some extent because of nonideal optical components. In an imaging system that is axially symmetric about an optical axis, Seidel aberrations such as spherical aberration, coma, field curvature, distortion, and astigmatism are common. Any aberration in the binary cell will distort the spot pattern as it is imaged between the SLM surface and the auxiliary focal plane. On multiple bounces the distortions can accumulate. Fortunately, because the beam divergence of the light and the pupil sizes in the binary cell system are relatively small, Seidel aberrations will be insignificant. This is also true because the spot pattern on both the SLM and the auxiliary focal planes are relatively small compared with the distances between optical components.

The main imaging problem in the binary cell arises because the system is not axially symmetric. Owing to this lack of symmetry configuration of the White cell, non-Seidel astigmatism will always be a critical issue. Because the beam in the White cell will never be at normal incidence to the surface of a spherical mirror, it is critical either to reduce the non-Seidel astigmatism or to compensate for it.

### A. Astigmatism Caused by White Cell Mirrors

Because the White cell mirrors B and C are tilted with respect to the optical axis, the images from the auxiliary focal plane to the SLM focal plane will accrue a particular amount of astigmatic aberration. Light propagating in the sagittal and tangential planes will experience different focal lengths. The astigmatism for a single reflection at a spherical surface is given as[10]

$$\frac{1}{d_o} + \frac{1}{d_{\mathrm{iT}}} = \frac{2}{R \cos\theta}, \tag{6}$$

$$\frac{1}{d_o} + \frac{1}{d_{\mathrm{iS}}} = \frac{2 \cos\theta}{R}, \tag{7}$$

where $d_o$ is the object distance, $d_{\mathrm{iT}}$ is the tangential image distance, and $d_{\mathrm{iS}}$ is the sagittal image distance measured along the chief ray; $R$ is the radius of curvature of the mirror, and $\theta$ is the angle of incidence of the chief ray. A comparison of Eqs. (6) and (7) with the basic lens equation,

$$\frac{1}{d_o} + \frac{1}{d_i} = \frac{1}{f}, \tag{8}$$

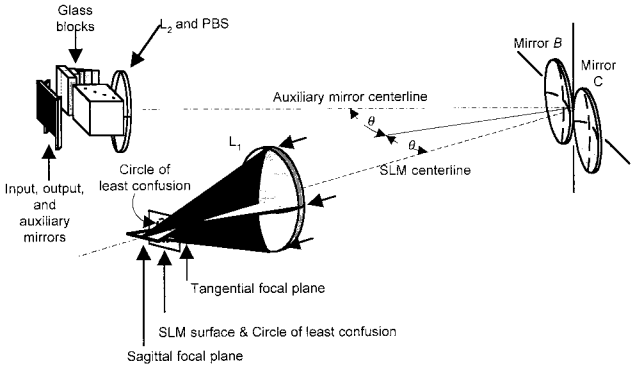


Fig. 5. Astigmatic focus at the plane of the SLM surface. The astigmatic image creates tangential and sagittal focal planes. The surface of the SLM is located in between these two focal planes at the circle of least confusion for best imaging.

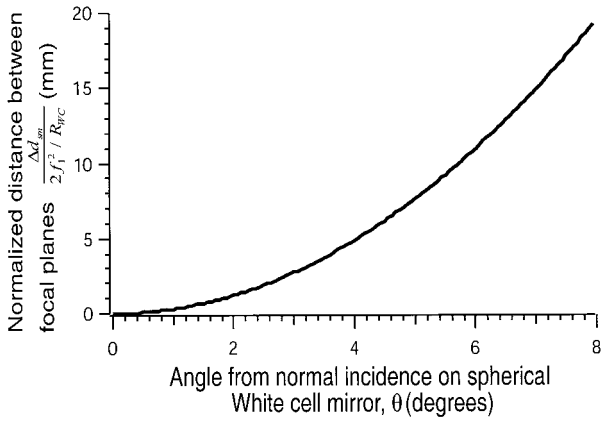


Fig. 6. Normalized astigmatism versus angle of incidence θ in the binary cell according to expression (14). The astigmatic image distance is normalized to $R_{WC}/2f_1^2$.

results in the effective focal lengths in the sagittal and tangential directions:

$$f_T = \frac{R\cos\theta}{2}, \tag{9}$$

$$f_S = \frac{R}{2\cos\theta}. \tag{10}$$

The astigmatism caused by the spherical mirrors will distort the imaging between the auxiliary focal plane and the face of the SLM. According to the first imaging condition of the new binary cell, the radii of curvature of mirrors B and C were chosen to properly image the SLM pixel array to the auxiliary focal plane and vice versa. Because input spots are introduced at the auxiliary focal plane, the astigmatism of the spherical mirrors will give rise to two separate focal planes in the SLM branch of the binary cell. This can be seen in Fig. 5. The tangential and sagittal focal planes are located along the optical axis in front of and behind the SLM surface, respectively. To achieve the sharpest focus, one must locate the SLM surface between the two focal planes near the circle of least confusion. Ideally, the distance between the two focal planes should be less than the depth of focus of the spots on the SLM.

Note that the angle θ in Fig. 5 is not exactly the angle of incidence that the chief ray makes on mirrors B and C. The angle shown in the figure is that between the SLM centerline and the auxiliary mirror centerline. For the design parameters and dimensions that we will eventually choose (in Section 5), however, the angle θ will be equivalent to the angle of incidence for all practical analyses. In addition, the maximum divergence of the beam is much smaller than the angle θ. Therefore the astigmatism analysis will be based solely on the lines that formed the angle θ.

The astigmatism in one pass through the binary cell can be calculated analytically by using the imaging conditions. As determined earlier, the distance $d_{sm}$ between the SLM and lens $L_1$ (disregarding astigmatism) is given by Eq. (2). With the astigmatism from one reflection of mirror B, however, two different distances are derived for where the SLM should be, one for the tangential focus and another for the sagittal focus. The distance between the SLM and $L_1$ for the tangential and sagittal focal planes are given, respectively, as

$$d_{sm\_t} = \frac{f_1}{f_2^2}(f_1 f_2 - f_1 d_{aux} + f_2^2) - \frac{2f_1^2}{R_{WC}\cos\theta}, \tag{11}$$

$$d_{sm\_s} = \frac{f_1}{f_2^2}(f_1 f_2 - f_1 d_{aux} + f_2^2) - \frac{2f_1^2\cos\theta}{R_{WC}}. \tag{12}$$

The distance between the tangential and the sagittal focal planes is a common measure of astigmatism. In the binary cell, this distance is determined by subtracting Eqs. (11) and (12), yielding

$$\Delta d_{sm} = d_{sm\_t} - d_{sm\_s} = \frac{2f_1^2}{R_{WC}}\left(\frac{1}{\cos\theta} - \cos\theta\right), \tag{13}$$

$$\frac{\Delta d_{sm}}{2f_1^2/R_{WC}} = \left[1 + \frac{\theta^2}{2} - \left(1 - \frac{\theta^2}{2}\right)\right] \approx \theta^2. \tag{14}$$

The greater $\Delta d_{sm}$ is, the greater the astigmatism. Because in a White cell there are multiple bounces, the astigmatism will accumulate. Thus from expression (14) the angle of incidence must be as close to normal incidence as possible. Figure 6 shows a plot of the normalized distance $\Delta d_{sm}$ versus the angle. Once the number of bounces, and thus the maximum acceptable $\Delta d_{sm}$ is determined, this plot can be used to determine the maximum acceptable angle of incidence θ for the light beams on mirrors B and C.

### B. Depth of Focus

Our goal in the Section 4.A was to reduce the astigmatic aberration as much as possible. The astigmatism in the binary cell will cause significant imaging problems only when the total astigmatic image dis-

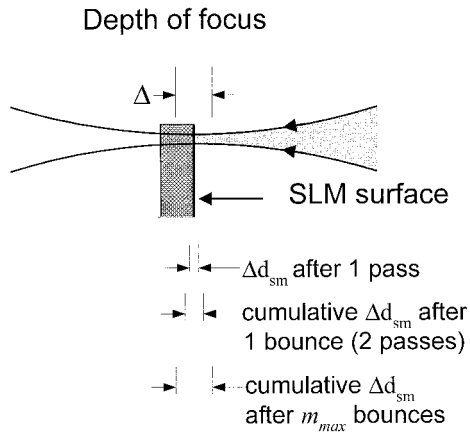


Fig. 7. Depth of focus due to beam divergence at the SLM surface. The depth of focus depends on the size of the beam waist as well as the wavelength of light. The astigmatic image distance $\Delta d_{\mathrm{sm}}$ after one, three, and $m_{\max}$ passes is also shown.

tance $\Delta d_{\mathrm{sm}}$ is longer than the depth of focus. The depth of focus is the distance along the optical axis over which the beam is focused as shown in Fig. 7. The depth of focus for our optical system that we are most interested in occurs at the SLM surface. For Gaussian beams the depth of focus is given as

$$\text{depth of focus} = 2\pi \frac{{w_0}^2}{\lambda}, \tag{15}$$

where $\lambda$ is the operating wavelength and $w_0$ is the beam-waist radius located on the surface of the SLM.

Figure 7 also shows the astigmatic image distance $\Delta d_{\mathrm{sm}}$ after one and two passes through the binary cell. Because the astigmatism occurs at each reflection from the White cell mirrors, the distance $\Delta d_{\mathrm{sm}}$ will accumulate with each pass. After a certain number of passes, the astigmatic image distance will become larger than the depth of focus. When this occurs, the spot on the SLM will become astigmatic.

The maximum number of passes, $m_{\max}$, that a beam can travel in the binary cell before it is significantly distorted is given as

$$m_{\max} = \frac{\Delta}{\Delta d_{\mathrm{sm}}}. \tag{16}$$

Combining Eqs. (15) and (16) yields the maximum allowable number of bounces:

$$m_{\max} = 2\pi \frac{{w_0}^2}{\Delta d_{\mathrm{sm}} \lambda}. \tag{17}$$

Next, we will discuss some strategies for handling the astigmatism.

### C. Reduction of Astigmatism in the Binary White Cell

According to Eq. (13), the astigmatism of the binary cell depends on the focal length $f_1$ of lens $L_1$, the radius of curvature of the White cell mirrors $R_{\mathrm{WC}}$, and the angle of incidence $\theta$ that the chief ray makes with the White cell mirrors.

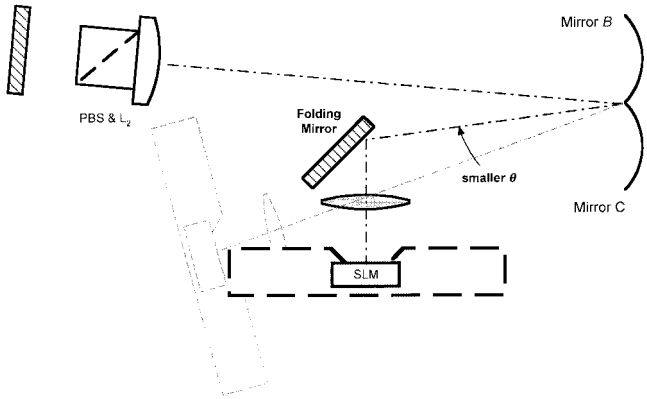


Fig. 8. Top view of the binary cell with a flat mirror to fold the path of the SLM branch. Folding the light path will allow us to reduce the angle of incidence $\theta$ on the White cell mirrors B and C.

The simplest way to reduce the astigmatism is to decrease the angle of incidence $\theta$ on the White cell mirrors. There are two techniques that we will use to reduce the angle of incidence on the White cell mirrors. The first technique uses a flat mirror to bend the SLM branch away from the light path of the auxiliary mirror branch. Figure 8 shows the top view of the binary cell with a flat folding mirror. The figure shows that the original angle was limiting by the SLM housing, which in our laboratory is significantly larger than the SLM active area. As seen in the figure, the angle $\theta$ can be reduced with the folding mirror to the extent that the folding mirror does not obstruct the beam path.

To understand the second technique for reducing $\theta$, we show in Fig. 9(a) a perspective view of the binary cell using a flat folding mirror as discussed earlier.

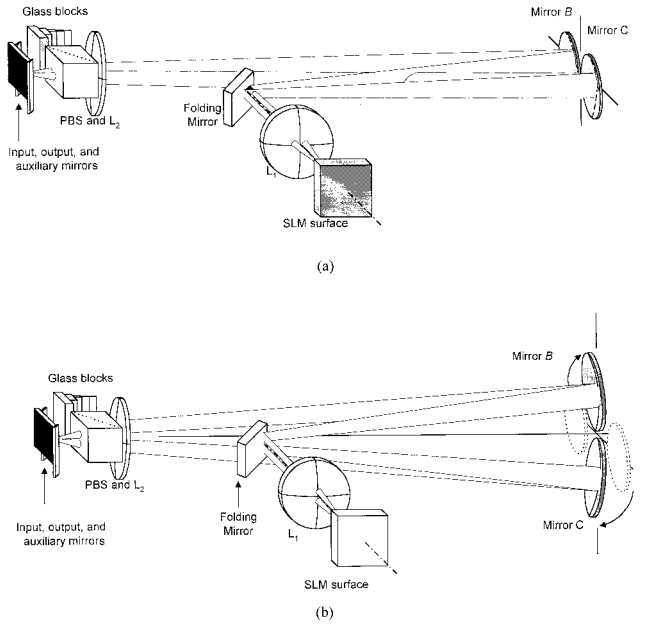


Fig. 9. Three-dimensional view of a binary White cell (a) with a folding mirror and (b) vertically oriented mirrors B and C.

As seen in this figure, the beam path for the auxiliary mirror branch passes behind the folding mirror.

We now decrease the incident angle further by reorienting the White cell mirrors to change the beam path. The White cell mirrors can be positioned vertically, one above the other with respect to the optical table, without affecting the imaging conditions. Figure 9(b) shows this change. If mirrors B and C are oriented vertically, then the beam path will be changed such that the angle of incidence can be reduced further. This design change will not affect the imaging of the White cell in that the spacing of the spot pattern is determined by the location of the centers of curvature of mirrors B and C (as opposed to the locations of the mirrors themselves).

### D. Correction of Astigmatism by Use of Astigmatic Mirrors

Using the techniques described above, we have seen how to decrease astigmatism by reducing the angle of incidence on the White cell mirrors. To fully correct the astigmatism in the White cell, however, it is necessary to have astigmatic mirrors for mirrors B and C. The astigmatism of the mirrors must compensate for the astigmatism caused by the angle of incidence.

The most straightforward approach to compensate for astigmatism is to use mirrors that have different radii of curvature in the $x$ and $y$ directions. From Eqs. (9) and (10) we know that the focal planes for sagittal and tangential rays are different for spherical mirrors. If we assume that radii of curvature of the mirrors are different in the tangential and sagittal planes, then we can obtain a relationship between the two radii by equating these two equations. Combining these equations yields

$$R_{\mathrm{WC\_S}} = R_{\mathrm{WC\_T}} \cos^2(\theta), \tag{18}$$

where $R_{\mathrm{WC\_S}}$ and $R_{\mathrm{WC\_T}}$ are the radii of curvature in the sagittal and tangential planes, respectively. Although fabricating such mirrors is possible, it is expensive.

A lower-cost approach is to create an equivalent astigmatic mirror by using a cylindrical lens just in front of mirrors B and C in the binary cell as shown in Fig. 10. Inserting a convex cylindrical lens into the binary cell will not significantly affect the tangential focus but will refract the sagittal rays. The cylindrical lens must be placed near the White cell mirrors, however, so as not to interfere with the first and second imaging requirements.

The proper focal length of the cylindrical lens must be chosen to fully correct the astigmatism in the binary cell. To accomplish this, we equate the two optical systems experienced by the tangential and sagittal rays. The tangential rays will be affected only by the spherical mirror, whereas the orthogonal sagittal rays will be bent by both the spherical mirror and the cylindrical lens. Equating the two optical

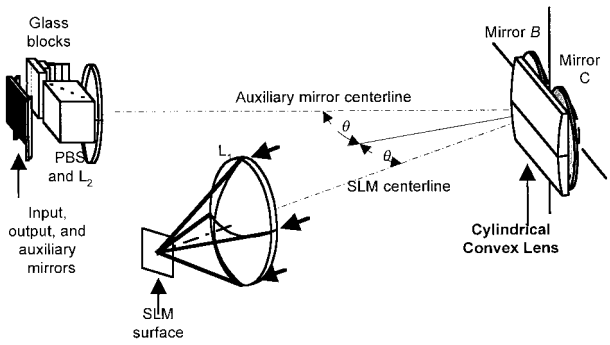


Fig. 10. Three-dimensional view of a binary White cell with a cylindrical mirror to compensate for non-Seidel astigmatism.

systems yields the following equation relating the focal lengths,

$$\frac{1}{f_T} = \frac{1}{f_S} + \frac{2}{f_{\mathrm{CYL}}}, \tag{19}$$

where $f_{\mathrm{CYL}}$ is the focal length of the cylindrical lens. The term containing the $f_{\mathrm{CYL}}$ is doubled because a beam will pass through the cylindrical lens two times for each reflection from the White cell mirrors.

Substituting Eqs. (9) and (10) into Eq. (19) and solving for the focal length of the cylindrical lens yields

$$f_{\mathrm{CYL}} = \frac{R\,\cos(\theta)}{\sin^2(\theta)}. \tag{20}$$

Figure 11 shows the focal length of the cylindrical lens needed to fully compensate for the astigmatism in the binary cell with a particular angle of incidence, θ. Choosing a cylindrical lens with the proper focal length according to the graph will bend the sagittal rays to a focus at the tangential focal plane. Ulti-

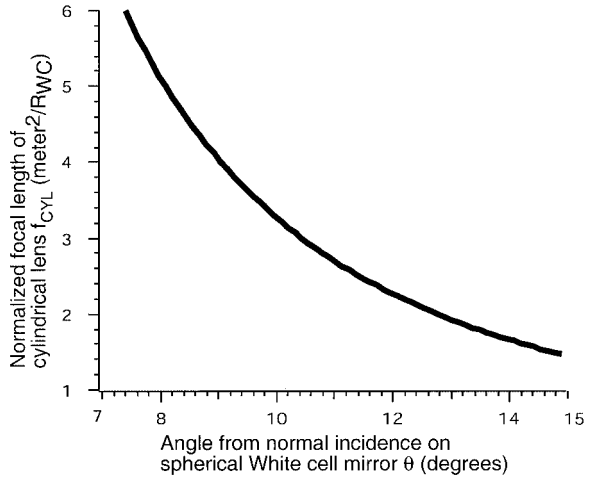


Fig. 11. Normalized focal length of the cylindrical lens needed to correct for the astigmatism as a function of the angle of incidence on the White cell (spherical) mirrors, θ. The focal length in this plot is normalized by dividing by the radius of curvature $R_{\mathrm{WC}}$ of the White cell mirrors.

mately, this will perfectly image the auxiliary mirror plane onto the surface of the SLM.

### 5. Numerical Example

In this section we give a specific design for a binary OTTD device. We will show how folding the path and modifying the White cell mirror placement (mirrors B and C) will reduce the astigmatism. Then we will indicate how to correct the astigmatism by using a cylindrical lens.

We take the SLM to be a liquid-crystal-type 16 × 16 array of pixels, each 100 μm square and on a 250-μm pitch. Thus the total image size of the SLM active area is 4 mm square. The housing for this device becomes important because it will put a lower limit on the angle θ in the unfolded device of Fig. 4. We therefore base our example on an actual SLM made by Boulder Nonlinear Optics, whose housing is 3 1/4 in. wide and 1 in. deep (1 in. = 2.54 cm). We take the individual spots to be Gaussian beams of a 25-μm beam waist, at a wavelength of 633 nm.

We use the imaging conditions of Section 4 to calculate lens and mirror positions and focal lengths.

Recall that there was an advantage to magnifying the image of the SLM onto the auxiliary mirror (Section 4). For our design, a magnification of $M = 1.66$ was chosen. For a time-delay increment of $\Delta = 1$ ps, this magnification will allow us to produce 7 bits of delays by using glass blocks, whereas only 5 bits could be achieved without significant truncation loss with a magnification of 1.00.

We then choose the distance $d_x$ between the auxiliary mirror and the beam splitter to be 40.0 mm, large enough for the input and output beams to enter and exit the cell without striking the other components. In addition, we would like to have the distance between the SLM and lens $L_1$ to be relatively short to capture as much of the light as possible. Unfortunately, we are limited to a minimum distance $d_{\mathrm{sm}}$ by the SLM housing and mounting apparatus. To compromise between maximum light collection and fixturing constraints, we design for a length of 15 to 30 mm between the SLM and lens $L_1$.

The imaging equations developed in Section 4 were based on ray matrices, which can be applied to Gaussian beams as long as the condition

$$\frac{k{w_0}^2}{2} \ll z \tag{21}$$

is satisfied, where $k$ is the wave number, $w_0$ is the Gaussian spot size, and $z$ is any arbitrary distance along the optical axis. The minimum distance $z$ along the optical axis is

$$\frac{k{w_0}^2}{2} = \left(\frac{2\pi}{633\ \mathrm{nm}}\right)\frac{(25\ \mu\mathrm{m})^2}{2} = 3.1\ \mathrm{mm} \ll z. \tag{22}$$

Therefore, because our desired distance $d_{\mathrm{sm}}$ between the SLM and lens $L_1$ is larger than 3.1 mm, the shortest propagation distance in our apparatus, our ray-matrix analysis is justified.

**Table 1. Design Parameters of the Binary White Cell TTD Switching Engine**

| Reference Label | Distances (mm) |
|---|---|
| $f_1$ | 299.9[a] |
| $f_2$ | 499.9[a] |
| $R_{\mathrm{WC}}$ | 412.4 |
| $d_1$ | 299.9 |
| $d_2$ | 499.9 |
| $d_x$ | 40.0 |
| $d_{bs}$[b] | 12.7 |
| $d_{\mathrm{sm}}$ | 25.34 |
| $M = -f_2/f_1$ | −1.667 |

[a]Nominal focal lengths for $f_1$ and $f_2$ are 300 and 500 mm, respectively.
[b]Thickness of the polarizing beam splitter.

By use of Eqs. (2)–(5), the focal lengths of the two lenses and the radius of curvature of the White cell mirrors are chosen for a desired magnification and range of distance $d_{\mathrm{sm}}$. Table 1 shows the initial design parameters of a binary cell that match our design requirements. Figure 12 shows the apparatus. The angle θ must be large enough such that the SLM housing and mounting apparatus that surrounds it (dashed line in Fig. 12) do not obstruct the beam path along the auxiliary mirror branch. For this unfolded binary cell design, the angle θ is approximately 7.5°.

Figure 13 characterizes the astigmatism caused by the traveling through one pass through the binary cell system that uses the optical components listed in Table 1. The astigmatic aberration, $\Delta d_{\mathrm{sm}}$, between these two image planes is 7.50 mm for θ equal to 7.5°. This astigmatic image distance is unacceptable especially in that the astigmatism will be compounded with every reflection from the White cell mirrors.

By folding the path as shown in Fig. 9(a), we can reduce the angle of incidence to 3°. This step alone reduces $\Delta d_{\mathrm{sm}}$ from 7.5 to 1.2 mm. By folding the path and rearranging the White cell mirrors as in Fig. 9(b), we reduce the angle of incidence θ further, to 1.0°. This significantly reduces the distance between the astigmatic focal planes $\Delta d_{\mathrm{sm}}$, from 7.50 to 0.133 mm. Using a folded mirror and reorienting the spherical mirrors in the binary cell will therefore reduce the astigmatism by 98.2%.

Figure 14 shows an Optics Software for Layout and Optimization (OSLO) simulation of the device of Table 1 for the three angles (a) θ = 7.5°, (b) θ = 3°, and (c) θ = 1°. On the right in each figure is the ray trace, and on the left is a field plot of the astigmatism. The horizontal axis is the distance along the optical axis in the vicinity of the image, and the vertical axis shows the location of the sagittal and tangential foci as a function of the distance of the original object from the optical axis, as a fraction of the object plane size. The units are millimeters. The astigmatism is found from the distance between the tangential and the sagittal foci on the horizontal axis. Table 2 shows the astigmatism $\Delta d_{\mathrm{sm}}$ as calculated by OSLO, which shows good agreement with the results obtained by using Eq. (13).

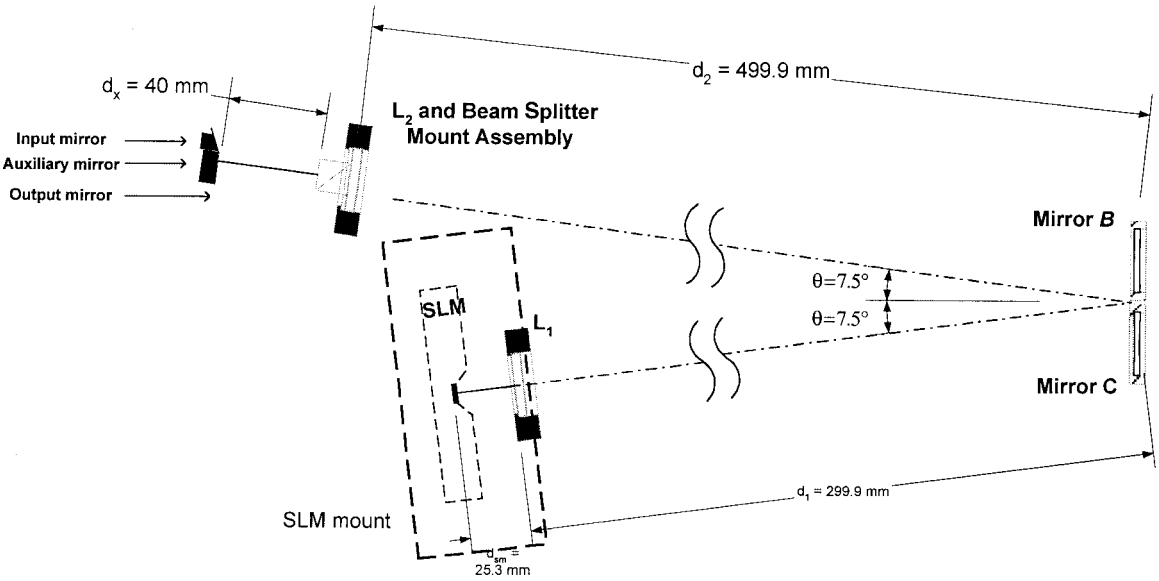


Fig. 12. Design configuration of binary cell TTD controller of the design of Table 1. Note that the SLM surface is embedded deep within the SLM housing (heavy dashed line), making it physically impossible to place the turning mirrors in the same plane as the SLM surface.

For a 25-μm-diameter Gaussian beam, the depth of focus is, from Eq. (15), equal to 1.55 mm. Thus Eq. (16) indicates that the maximum number of bounces is approximately 12. Thus, from an astigmatism point of view, one can produce 6 bits of delay with this design.

Alternatively, one can correct the astigmatism rather than simply try to avoid it. For our original angle $\theta = 7.5°$, a cylindrical lens with a focal length of $f_{\mathrm{CYL}} = 24$ m will correct the astigmatism. This is verified in the OSLO simulation of Fig. 15. The angle of incidence on the spherical mirror is 7.5°. The astigmatism for an object on the axis (the horizontal axis of the plot in Fig. 15), $\Delta d_{\mathrm{sm}}$, is now reduced to 0.00144 mm. Note that, with the cylindrical lens, the worst case (an object at the edge of the input plane, corresponding to the top of the plot) is $\Delta d_{\mathrm{sm}} = 1.80$ mm, approximately four times better than the best case of the uncorrected White cell.

The cylindrical lens has a focal length of 24 m in this example, but it is not a practical value. One is now at liberty, however, to increase θ until a suitable standard lens is found. For example, a standard cylindrical lens of focal length 10.0 m could be used to completely correct the astigmatism if the angle of incidence is increased to 11.77°. With either method, the number of bounces in this case is no longer limited by astigmatism because the astigmatism is, in theory, corrected on every bounce. The bounce number will be still limited by loss and the SLM space–bandwidth product.

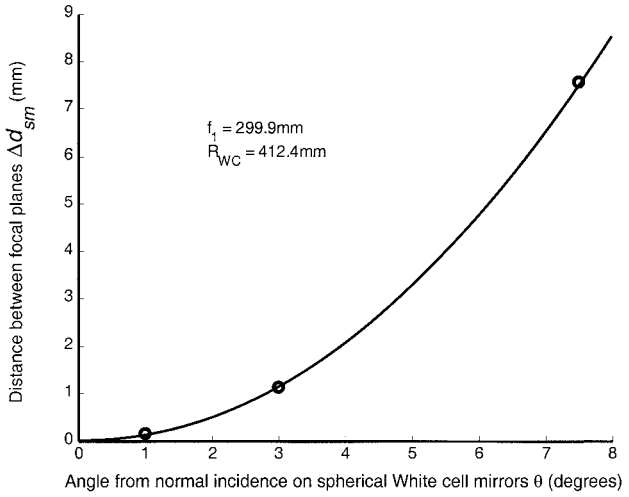


Fig. 13. Astigmatism versus angle of incidence θ in the binary bell of the design of Table 1. The circled data points on the graph denote $\Delta d_{\mathrm{sm}}$ for the angles 7.5°, 3°, and 1°.

## 6. Summary and Conclusions

We have proposed a new configuration for a binary-style optical true-time-delay device based on the White cell. The term "binary" means that the number of delays is proportional to the number of bounces raised to the power of 2. This means that this configuration results in more delays for a given number of bounces than the designs described in Ref. 7. That, in turn, means lower loss. A large number of light beams can circulate in the White cell simultaneously. Because in a phased-array radar there is one light beam for each antenna element or subarray, a single White cell device can support a large array with thousands of elements. In addition, because the White cell approach can produce 16 or more bits of delay, the steering resolution for the radar can be high.

The earlier binary White cell–based TTD design used a liquid-crystal SLM that required a SLM, a polarizing beam splitter, two lenses, and four spher-

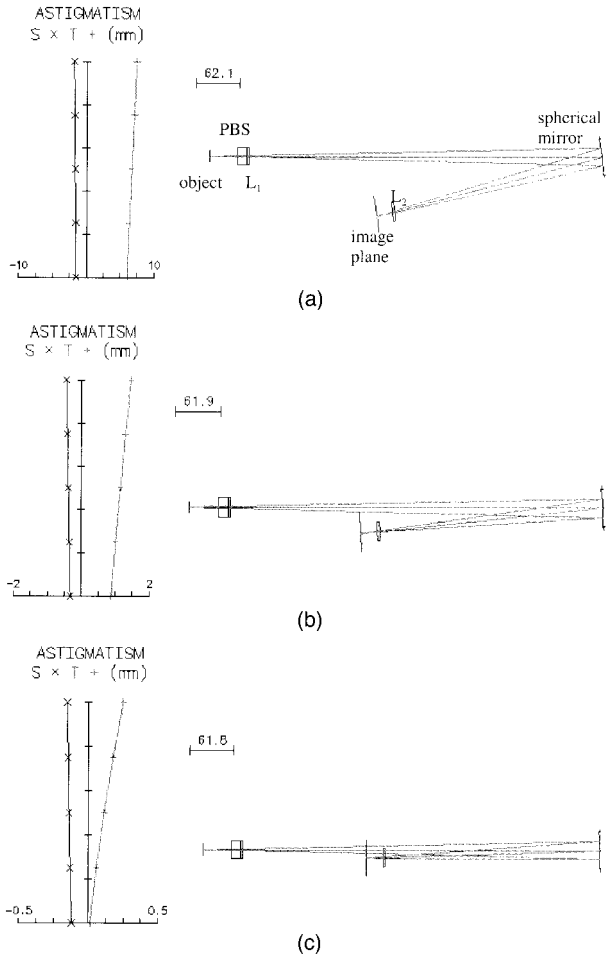


Fig. 14. Simulations in OSLO showing the reduction in astigmatism as the angle is decreased. The optical system parameters are those of Table 1. On the left side of each figure is a plot showing the sagittal (×) and tangential (+) foci. The vertical axis is the position of the original object with respect to the optical axis, as a fraction of the object plane size (maximum is 1). The horizontal axis is the distance (in millimeters) along the optical axis in the vicinity of the image (this axis is tipped at 2θ). The bars indicate the scale in millimeters. (a) θ = 7.5°, (b) θ = 3°, (c) θ = 1°. The astigmatism is the difference between the two curves on the horizontal axis. Note the differences in the scale on the horizontal axes of the plots.

ical mirrors (in addition to the delay elements). The new design removes two spherical mirrors. This is achieved by moving the polarizing beam splitter away from the SLM, effectively putting the path selection function at one end of the White cell while actual path switching is done at the other. Previously, selection and switching were done in the same location, and two White cells were required. The new arrangement also has the advantage of allowing magnification of the spot pattern on the delay elements, reducing divergence and increasing the length of delays that can be produced by use of glass blocks.

We also analyzed the astigmatism in this new binary cell. Two methods were discussed to correct for the astigmatism in the binary cell by reducing the angle of incidence on the White cell mirrors. This

**Table 2. Sagittal and Tangential Foci and Astigmatism $\Delta d_{sm}$ as a Function of the Angle in the White Cell Whose Parameters Are Listed in Table 1[a]**

| Angle of White cell | Sagittal Focus (OSLO) | Tangential Focus (OSLO) | $\Delta d_{sm}$ (OSLO) | $\Delta d_{sm}$ [Eq. (13)] |
|---|---|---|---|---|
| 7.5° | 6.063608 | −1.471687 | 7.535295 | 7.50 |
| 3° | 0.883637 | −0.315539 | 1.199176 | 1.2 |
| 1° | 0.012009 | −0.121129 | 0.133138 | 0.133 |

[a]All units are in millimeters.

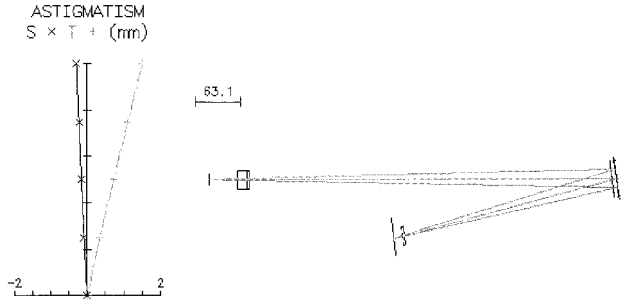


Fig. 15. Cylindrical lens is placed in front of the spherical mirror to correct the astigmatism. The focal length is $f_{CYL} = 24$ m for θ = 7.5°. The astigmatism for an object on axis is now 0.00144 mm.

was done by first using a flat mirror to fold the optical path to the SLM. Then the White cell mirrors B and C are stacked one above the other, which reduces the angle of incidence even further.

Alternatively, a convex cylindrical lens was used to rectify the astigmatism. When placed in front of the White cell mirrors, the cylindrical lens compensates for the astigmatism by bending the sagittal rays. Using the proper focal length for this lens fully corrects the astigmatism between the auxiliary conjugate plane and the SLM surface.

Finally, we presented a specific design for the binary White cell switching engine. The delay elements and their detailed design will be reported on elsewhere. In the switching engine, if the distance between the sagittal and tangential focal planes is used as the measure of the astigmatism, the astigmatism was reduced from 7.6 to 1.2 mm by folding the path and reduced further to 0.13 mm by stacking the spherical mirrors. The total astigmatism accumulated in $m$ bounces should not exceed the depth of focus, which for our design was 1.55 mm. This limits the uncorrected design to 12 bounces, or 6 bits of delay (64 delays). By use of an appropriate cylindrical lens, the astigmatism can be eliminated entirely. A convex cylindrical lens with a focal length of 24.0 m placed directly in front of the White cell mirrors will fully compensate for the astigmatism in the 7.5° (unfolded) binary cell. In this case, the number of bounces is limited by the loss that can be tolerated and the space–bandwidth product of the SLM.

The authors acknowledge Stuart A. Collins, Jr., who originally invented the binary White cell OTTDs

and who provided much technical help during the execution of this work.

## References

1. H. Zmuda and E. N. Toughlian, "Photonic aspects of modern radar," in *The Artech House Optoelectronics Library*, B. Culshaw, A. Rogers, and H. Taylor, eds. (Artech House, Norwood, Mass., 1994), p. 550.
2. K. P. Jackson, S. A. Newton, B. Moslehi, M. Tur, C. C. Cutler, J. W. Goodman, and H. J. Shaw, "Optical fiber delay-line signal processing," IEEE Trans. Microwave Theory Techn. **MTT-33,** 193–209 (1985).
3. S. Sales, J. Pampany, J. Martí, and D. Pastor, "Solutions to the synthesis problem of optical delay line filters," Opt. Lett. **20,** 2438–2440 (1995).
4. J. White, "Long optical paths of large aperture," J. Opt. Soc. Am. **32,** 285–288 (1942).
5. J. U. White, "Very long optical paths in air," J. Opt. Soc. Am. **66,** 411–416 (1976).
6. B. L. Anderson and C. D. Liddle, "Optical true time delay for phased-array antennas: demonstration of a quadratic White cell," Appl. Opt. **41,** 4912–4921 (2002).
7. B. L. Anderson and R. Mital, "Polynomial-based optical true-time delay devices with microelectromechanical mirror arrays," Appl. Opt. **41,** 5449–5461 (2002).
8. S. A. Collins, Jr. and B. L. Anderson, "Device and method for producing optically-controlled incremental time delays," U.S. patent 6,388,615 (14 May 2002).
9. B. L. Anderson, S. A. Collins, Jr., C. A. Klein, E. A. Beecher, and S. B. Brown, "Optically produced true-time delays for phased antenna arrays," Appl. Opt. **36,** 8493–8503 (1997).
10. T. H. Edwards, "Multiple-traverse absorption cell design," J. Opt. Soc. Am. **51,** 98–102 (1961).